Hindawi
Mathematical Problems in Engineering
Volume 2019, Article ID 9867467, 13 pages
https://doi.org/10.1155/2019/9867467

Research Article

Improved Linear Active Disturbance Rejection Control for Lever-Type Electric Erection System with Varying Loads and Low-Resolution Encoder

Hailong Niu, Qinhe Gao, Zhihao Liu, Shengjin Tang, and Wenliang Guan

Xi'an High Technology Institute, Xi'an 710025, China

Correspondence should be addressed to Qinhe Gao; qhgao201@126.com

Received 2 November 2018; Accepted 12 December 2018; Published 17 January 2019

Academic Editor: Rafael Morales

The lever-type electric erection system is a novel kind of erection system and the experimental platform in this paper operates with varying loads and low-resolution encoder. For high accuracy trajectory tracking, linear active disturbance rejection control (LADRC) is introduced. An approximate model, consisting of the servo system configured at velocity control mode and the lever-type erection mechanism, is built by means of system identification and curve fitting. Reduced-order LADRC based on the further simplified model is proposed to improve tracking accuracy and robustness. As comparisons, traditional LADRC and PID with high-gain tracking differentiator (HGTD) are designed. Simulation and experimental results indicate that reduced-order LADRC can realize higher trajectory tracking accuracy with low-resolution encoder and has better robustness to variation in erection loads, compared with traditional LADRC and PID with HGTD.

1. Introduction

The erection system is an important component of weaponry and engineering machinery, such as the rocket launcher and the dump truck. Typically, the erection system needs to track the planned trajectory. However, the trajectory tracking accuracy could be affected by variation in erection loads, resolution of sensors, and other disturbances. Uncertainties always exist in physical servo system and affect the tracking accuracy. Many nonlinear control methods are developed to achieve high accuracy trajectory tracking, such as the adaptive integral robust controller [1], the adaptive backstepping controller with modified LuGre model [2], and the adaptive repetitive controller [3].

Traditional erection systems are usually hydraulically driven by multistage hydraulic cylinder, which has long strokes and shock during the process of changing stage. Time-varying integral adaptive sliding mode control [4] and flow-pressure compound control [5] have been adopted to control the hydraulic erection system. With the improvement of servo motor and drive mechanism, the electric cylinder can be used as the actuator in the electric erection system [6]. The erection system in this paper combines the single-stage electric cylinder with the lever-type erection mechanism, which can shorten the strokes and avoid shock. Considering the modeling uncertainties, varying loads, and low-resolution encoder of the experimental platform in this paper, traditional linear controllers are difficult to satisfy the performance demands in terms of tracking accuracy and robustness. Therefore, linear active disturbance rejection control (LADRC) is introduced.

The concept of active disturbance rejection control (ADRC) was firstly proposed by Han [7], which inherits from classic PID and has better performance in rejecting the disturbances actively [8]. The core of ADRC is estimating the generalized disturbances, consisting of internal model uncertainties and external disturbances, and compensating for them, such that a relatively low precision model is necessary to design the control loop [9, 10]. The normal ADRC consists of tracking differentiator (TD), extended state observer (ESO), nonlinear state error feedback (NLSEF), and disturbance rejection (DR) [11]. Gao [12] developed LADRC, which is the simplification of ADRC by using linear extended state observer (LESO) and linear state error feedback (LSEF).

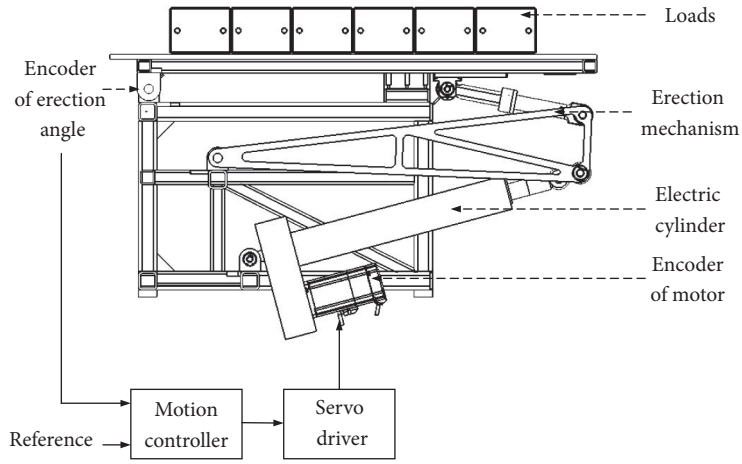

Figure 1: Composition of the electric erection system.

LADRC has fewer parameters and is easily tuned in practice. The convergence and stability of LADRC have been proved in time domain [13, 14] and frequency domain [15] [16]. The validity has been verified in many applications [17–21]. Consequently, LADRC has theoretical completeness and practicability.

First, this paper builds an approximate model of the electric erection system, which is composed of the servo system configured at velocity control mode and the lever-type erection mechanism. Second, reduced-order LADRC is proposed based on further simplified model. As comparisons, traditional LADRC and PID with high-gain tracking differentiator (HGTD) are designed for this system. Finally, simulations and experiments are carried out to validate the effectiveness and robustness of the proposed controllers.

The rest of this paper is organized as follows. Section 2 describes the composition of the electric erection system and the experimental platform. Section 3 builds the approximate model of the erection system. Section 4 designs reduced-order LADRC, traditional LADRC, and PID with HGTD for the erection system. Section 5 conducts the simulation and experimental verification. The conclusions are given in Section 6.

2. System Introduction

The electric erection system is a typical mechatronic servo system, which mainly consists of a controller, a servo driver, an electric cylinder, an erection mechanism, loads, and encoders, as shown in Figure 1.

The motion controller acquires the signals of encoders and calculates the control signal according to the control algorithm. The servo driver is configured at velocity control mode and controls the speed of servo motor in response to the analog voltage command of -10–+10 V. The electric cylinder can make rotation motion of the servo motor to linear motion of the pushrod via the reducer and ball screw and then thrust the erection mechanism and loads. The erection angle and the motor rotation angle are detected by encoders and transmitted to the controller.

Figure 2 shows the experimental platform of the electric erection system. The motion controller in IPC is GTS800, produced by Googoltech®, and the servo driver is MCDKT3520CA1, produced by Panasonic®. The encoder of erection angle, produced by Tamagawa®, outputs pulse signals with the resolution of 0.05°. The erection loads are adjustable from zero mass block (30 kg) to six mass blocks (180 kg).

3. Modeling of Electric Erection System

The electric erection system is a position servo system with the speed command of the servo driver as input and the erection angle as output. The control block diagram of the electric erection system is shown in Figure 3.

The servo driver and the servo motor can be considered as a whole and called the servo system. Therefore, the approximate model of the electric erection consists of two parts—the servo system and the erection mechanism.

3.1. Servo System Model. Figure 4 shows the control block diagram of the servo system.

The commercial servo driver, which is configured at velocity control mode, has inner velocity controller and current controller. Some parameters of the controllers and servo motor are not public. Also, there are some uncertainties, such as friction, parameter variation, and delay. So it is difficult to build a precise model of the servo system.

Typically, an approximate second-order model is devoted to describe the velocity loop of the servo system [19] and the transfer function can be described as

$$G(s) = \frac{\Theta_m(s)}{U(s)} = \frac{K}{s(Ts+1)} \quad (1)$$

where $\Theta_m(s)$ and $U(s)$ are Laplace transform of the motor rotation angle θ_m and the speed command u, respectively, K is the transfer coefficient, and T is the time constant.

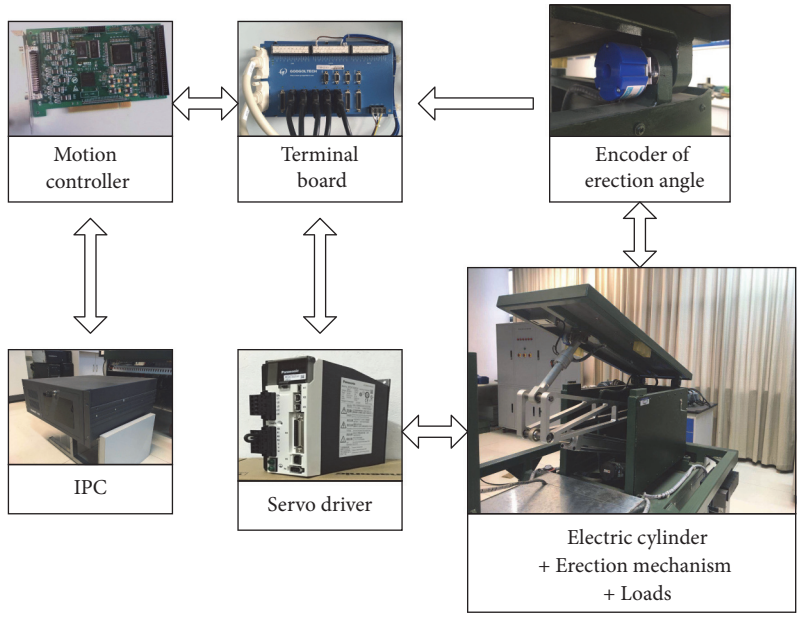

Figure 2: Experimental platform of the electric erection system.

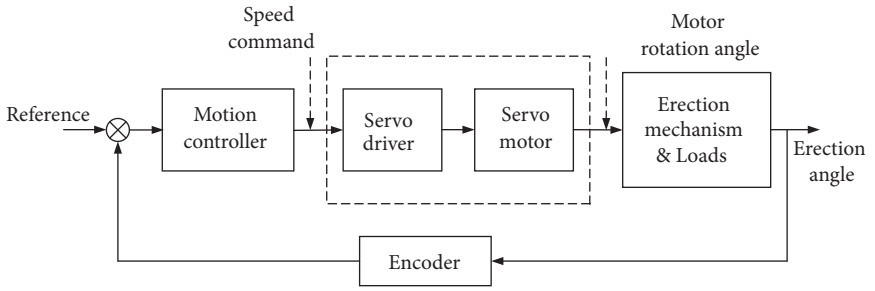

Figure 3: Control block diagram of the electric erection system.

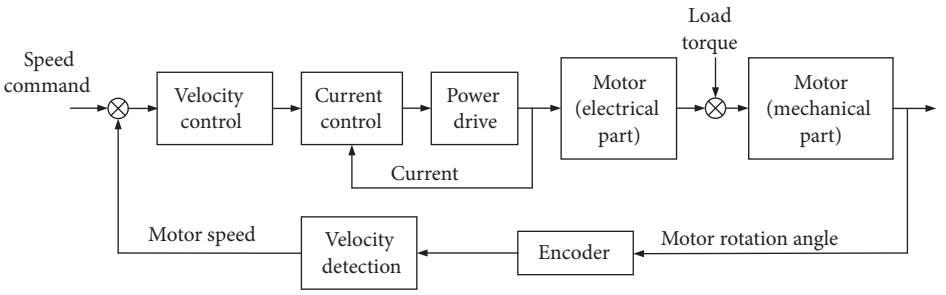

Figure 4: Control block diagram of the servo system.

In order to identify the model parameters, the step response method is applied to the servo system on the experimental platform. According to the input gain of speed command, the unit of speed command can be converted from V to r/min. Step response tests of 100, 200, 300, and 400 r/min are, respectively, carried out on the experimental platform. The output of the servo system is the motor rotation angle, with the unit of rad. The experimental curves are shown in Figure 5.

The model parameters can be identified by means of the system identification toolbox in MATLAB. The identification model of the servo system can be described as

$$G(s) = \frac{20.944}{s(0.0158s + 1)} \quad (2)$$

3.2. Erection Mechanism Model. The model of the erection mechanism takes the motor rotation angle θ_m as the input

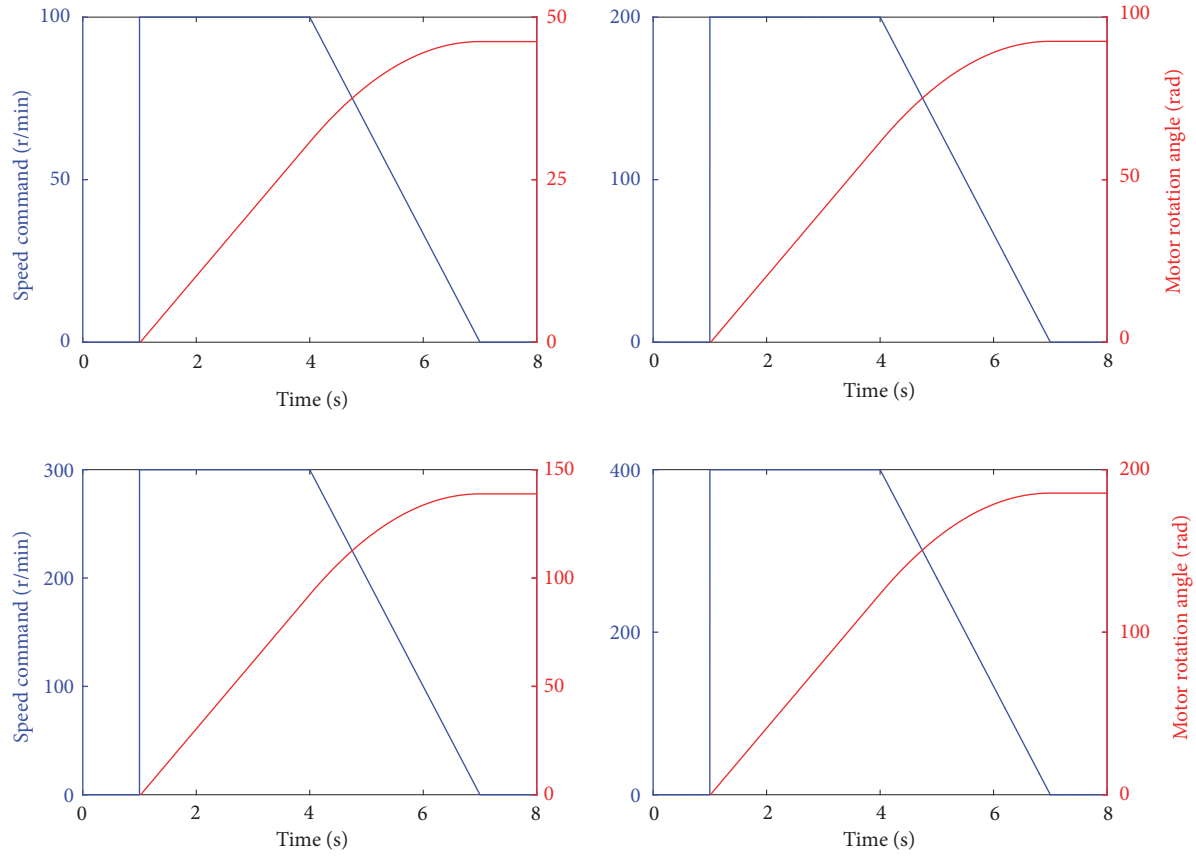

Figure 5: Step response curves of the servo system.

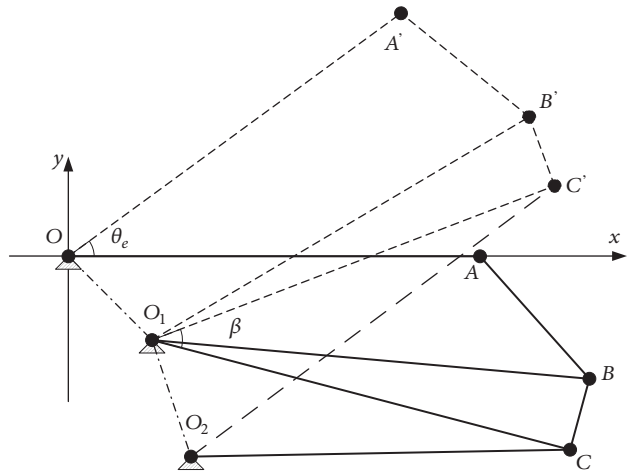

Figure 6: Structure of the lever-type mechanism.

and the erection angle θ_e as the output, consisting of the transmission mechanism in the electric cylinder and the lever-type mechanism.

The rigid model of transmission mechanism can be expressed as

$$S = \frac{\theta_m L}{2\pi i} \tag{3}$$

where S is the extended length of the pushrod, L is the lead of the ball screw, and i is the reduction ratio of the reducer.

The lever-type mechanism is composed of the electric cylinder O_2C, the triangular arm O_1BC, and the connecting rod AB, as shown in Figure 6. To analyze the kinematics of the lever-type mechanism, a coordinate system is established in the vertical plane through the center of gravity, where the origin O is the rotation center of the erection loads, the X axis is horizontal, and the Y axis is vertical.

Table 1: Values of structure size and initial coordinate.

Parameters/Units	Symbols	Values
Length of $O_1B(O_1B')$/m	$\left\|\overrightarrow{O_1B}\right\|\left(\left\|\overrightarrow{O_1B'}\right\|\right)$	0.8
Length of $O_1C(O_1C')$ /m	$\left\|\overrightarrow{O_1C}\right\|\left(\left\|\overrightarrow{O_1C'}\right\|\right)$	0.79
Length of $BC(B'C')$ /m	$\left\|\overrightarrow{BC}\right\|\left(\left\|\overrightarrow{B'C'}\right\|\right)$	0.1261
Length of $AB(A'B')$/m	$\left\|\overrightarrow{AB}\right\|\left(\left\|\overrightarrow{A'B'}\right\|\right)$	0.3
Coordinate of O /m	(x_o, y_o)	(0,0)
Coordinate of O_1 /m	(x_{o_1}, y_{o_1})	(0.15,-0.15)
Coordinate of O_2 /m	(x_{o_2}, y_{o_2})	(0.22,-0.37)
Coordinate of A /m	(x_A, y_A)	(0.75,0)
Coordinate of B /m	(x_B, y_B)	(0.9463,-0.2269)
Coordinate of C /m	(x_C, y_C)	(0.9146,-0.3489)
Initial length of electric cylinder/m	$\left\|\overrightarrow{O_2C}\right\|$	0.6949

When the extended length of the electric cylinder is S, points A, B, and C move to points A', B', and C', the triangular arm O_1BC turns the angle of β, and the erection angle is θ_e. In the initial position, S is zero and θ_e is zero. The structure size and the coordinate of points A, B, and C are shown in Table 1.

Ignoring the deformation of the mechanism, the kinematics analysis can be expressed as

$$\begin{aligned}
\left|\overrightarrow{O_2C'}\right| &= \left|\overrightarrow{O_2C}\right| + S \\
\cos\angle O_2O_1C &= \frac{\left|\overrightarrow{O_1O_2}\right|^2 + \left|\overrightarrow{O_1C}\right|^2 - \left|\overrightarrow{O_2C}\right|^2}{2\left|\overrightarrow{O_1O_2}\right| \cdot \left|\overrightarrow{O_1C}\right|} \\
\cos\angle O_2O_1C' &= \frac{\left|\overrightarrow{O_1O_2}\right|^2 + \left|\overrightarrow{O_1C'}\right|^2 - \left|\overrightarrow{O_2C'}\right|^2}{2\left|\overrightarrow{O_1O_2}\right| \cdot \left|\overrightarrow{O_1C'}\right|} \\
\beta &= \angle O_2O_1C' - \angle O_2O_1C \\
\begin{bmatrix} x_{B'} - x_{O_1} \\ y_{B'} - y_{O_1} \end{bmatrix} &= \begin{bmatrix} \cos\beta & -\sin\beta \\ \sin\beta & \cos\beta \end{bmatrix} \begin{bmatrix} x_B - x_{O_1} \\ y_B - y_{O_1} \end{bmatrix} \\
\begin{bmatrix} x_{A'} \\ y_{A'} \end{bmatrix} &= \begin{bmatrix} \cos\theta_e & -\sin\theta_e \\ \sin\theta_e & \cos\theta_e \end{bmatrix} \begin{bmatrix} x_A \\ y_A \end{bmatrix} \\
\left|\overrightarrow{A'B'}\right|^2 &= (x_{B'} - x_{A'})^2 + (y_{B'} - y_{A'})^2
\end{aligned} \tag{4}$$

Solving inverse trigonometric and quadratic equation, the expression of θ_e can be obtained as

$$\begin{aligned}
\theta_e &= \arccos\left(\frac{ac - b\sqrt{a^2 + b^2 - c^2}}{a^2 + b^2}\right) \\
a &= x_{B'} = \left(x_B - x_{O_1}\right)\cos\beta - \left(y_B - y_{O_1}\right)\sin\beta + x_{O_1} \\
b &= y_{B'} = \left(x_B - x_{O_1}\right)\sin\beta - \left(y_B - y_{O_1}\right)\cos\beta + y_{O_1} \\
c &= \frac{x_A^2 + x_{B'}^2 + y_{B'}^2 - \left|\overrightarrow{A'B'}\right|^2}{2x_A}
\end{aligned} \tag{5}$$

The relationship between θ_e and θ_m can be obtained based on (3) and (5). However, the analytical expression is complicated. It is not convenient for building the system model and designing the control algorithm. So an approximate polynomial expression [22] is used to express the relationship, which is obtained by means of curve fitting.

The maximum stroke of the electric cylinder is 0.3 m, the reduction ratio i is two, and the lead of ball screw L is 0.005 m. Changing S from 0 to 0.3, θ_m and θ_e can be calculated according to (3) and (5), respectively. Then, curve fitting is performed in MATLAB and the approximate polynomial expression is:

$$\begin{aligned}
\theta_e &= f(\theta_m) \\
&= 1.391 \times 10^{-9}\theta_m^3 - 5.863 \times 10^{-7}\theta_m^2 + 0.001763\theta_m \\
&\quad - 0.005364
\end{aligned} \tag{6}$$

where the units of θ_m and θ_e are both rad, the confidence bounds of the coefficients are 95%, the RMSE is 0.0049, and the SSE is 0.2419.

The calculated curve and fitted curve are shown in Figure 7.

3.3. System Model. Based on (1) and (6), the approximate model of the electric erection system can be expressed in the form of differential equation as

$$\frac{d^2\theta_e}{dt^2} = \left(\frac{d^2 f(\theta_m)/d\theta_m^2}{df(\theta_m)/d\theta_m} - 1\right)\frac{d\theta_e}{dt} + \frac{K}{T}\frac{df(\theta_m)}{d\theta_m}u \tag{7}$$

For the convenience of designing control algorithm, define the state variable $x_1 = \theta_e$ and $x_2 = \dot{\theta}_e$ and transform

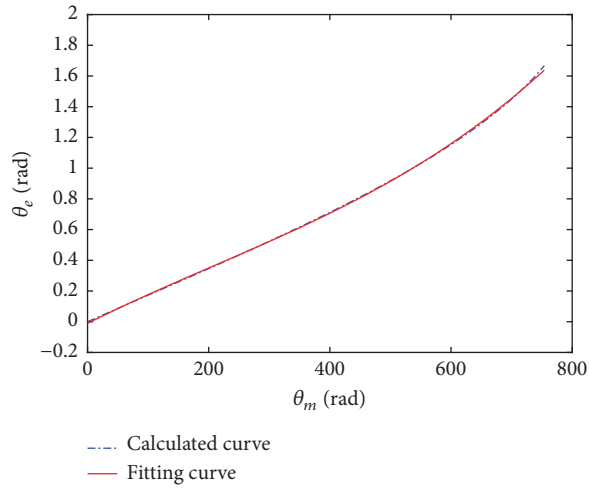

FIGURE 7: Curves of the relationship between θ_e and θ_m.

the differential equation to the state-space form. The system model is expressed as

$$\begin{aligned} \dot{x}_1 &= x_2 \\ \dot{x}_2 &= ax_2 + bu \\ y &= x_1 \end{aligned} \tag{8}$$

where a is the model parameter and b is the control gain. Their expressions are

$$\begin{aligned} a &= \frac{d^2 f(\theta_m)/d\theta_m^2}{df(\theta_m)/d\theta_m} - 1 \\ b &= \frac{K}{T}\frac{df(\theta_m)}{d\theta_m} \end{aligned} \tag{9}$$

4. Design of Control Algorithm

The control target is to let the electric erection system track the planned trajectory within the error range of $\pm 0.2^\circ$. However, there are several factors affecting the tracking accuracy as follows:

(1) There are model uncertainties between the actual system and the approximate model in previous section.

(2) There is variation in erection loads.

(3) The low-resolution encoder of erection angle outputs signals with quantization noise.

(4) There are other external disturbances during the process of erection.

In order to overcome above problems and realize the control target, LADRC is introduced to control the electric erection system, which has low requirements for the modeling precision and can estimate and compensate for the generalized disturbances.

4.1. Control System Structure. The normal LADRC consists of TD, LESO, LSEF, and DR. For the electric erection system, the suitable erection trajectory should be planned to improve the stability and rapidity of the erection process. The information of velocity and acceleration is easy to be obtained, so there is no need to use TD. LESO is used to estimate the state variables and the generalized disturbances, which is the core of LADRC. In order to improve tracking accuracy, LSEF is modified by combining state error feedback with velocity and acceleration feedforward. The structure of the control system is shown in Figure 8.

In this paper, half period cosine function is used to plan the erection trajectory, which is expressed as

$$\begin{aligned} \theta_r &= \frac{\theta}{2} - \frac{\theta}{2}\cos\left(\frac{\pi}{t_f}t\right) \\ \dot{\theta}_r &= \frac{\pi\theta}{2t_f}\sin\left(\frac{\pi}{t_f}t\right) \\ \ddot{\theta}_r &= \frac{\pi^2\theta}{2t_f^2}\cos\left(\frac{\pi}{t_f}t\right) \end{aligned} \tag{10}$$

where θ_r, $\dot{\theta}_r$, and $\ddot{\theta}_r$ are, respectively, the reference position, velocity, and acceleration at the moment of t, θ is the target position, and t_f is the duration of the erection process.

4.2. LADRC Design

4.2.1. Reduced-Order LADRC. For the servo system model (1), ignoring the dynamic characteristics of the velocity loop [23], the model can be further simplified as

$$G'(s) = \frac{\Theta_m(s)}{U(s)} = \frac{K}{s} \tag{11}$$

Besides, the extended state-space form of the simplified model can be expressed as

$$\begin{aligned} \dot{x}_1 &= x_2 + b_r u \\ \dot{x}_2 &= h \\ y &= x_1 \end{aligned} \tag{12}$$

$$b_r = K\frac{df(\theta_m)}{d\theta_m} \tag{13}$$

where x_2 is the generalized disturbances including model uncertainties and external disturbances, h is the differentiation of the generalized disturbances and b_r is the control gain.

The model uncertainties caused by the simplified model (12) can be estimated and compensated for by LADRC.

Structure the second-order LESO as

$$\begin{aligned} \dot{z}_y &= z_d + 2\omega_o\left(x_1 - z_y\right) + b_r u \\ \dot{z}_d &= \omega_o^2\left(x_1 - z_y\right) \end{aligned} \tag{14}$$

where z_y and z_d estimate x_1 and x_2, respectively, and ω_o is the observer gain.

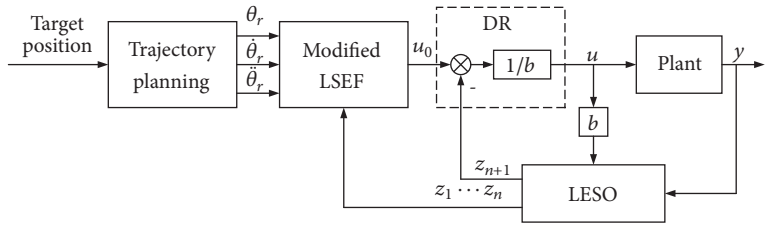

Figure 8: Structure of the control system.

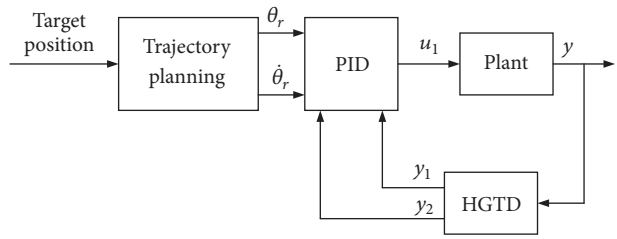

Figure 9: Structure of PID controller with HGTD.

With the estimation of the generalized disturbances, LADRC can compensate for them in real time as

$$u = \frac{u_0 - z_d}{b_r} \tag{15}$$

Although b_r varies with θ_m based on (13), the encoder of motor can accurately measure θ_m in real time and b_r can be calculated in real time.

The modified LSEF combines position error feedback with velocity and acceleration feedforward to improved tracking accuracy and stability, which is expressed as

$$u_0 = k_p\left(\theta_r - z_y\right) + k_v\dot{\theta}_r + k_a\ddot{\theta}_r \tag{16}$$

where k_p, k_v, and k_a are the coefficient of position error feedback, velocity feedforward, and acceleration feedforward, respectively.

4.2.2. Traditional LADRC. Based on the second-order system model (8), the third-order extended state-space representation can be expressed as

$$\begin{aligned} \dot{x}_1 &= x_2 \\ \dot{x}_2 &= x_3 + bu' \\ \dot{x}_3 &= h' \\ y &= x_1 \end{aligned} \tag{17}$$

where x_3 is the generalized disturbances and h' is the differentiation of the generalized disturbances.

The third-order LESO can be structured as

$$\begin{aligned} \dot{z}_1 &= z_2 + 3\omega_o'\left(x_1 - z_1\right) \\ \dot{z}_2 &= z_3 + 3\omega_o'^2\left(x_1 - z_1\right) + bu' \\ \dot{z}_3 &= \omega_o'^3\left(x_1 - z_1\right) \end{aligned} \tag{18}$$

where z_1, z_2, and z_3 estimate x_1, x_2, and x_3, respectively, and ω'_o is the observer gain.

The expressions of DR and modified LSEF are designed in the same way as (15) and (16), which are shown as

$$u' = \frac{u_0' - z_3}{b} \tag{19}$$

$$u_0 = k_p'\left(\theta_r - z_1\right) + k_v'\dot{\theta}_r + k_a'\ddot{\theta}_r \tag{20}$$

where k'_p, k'_v, and k'_a are the coefficient of position error feedback, velocity feedforward, and acceleration feedforward, respectively.

For both second-order and third-order LESO, if the differentiation of the generalized disturbances is bounded, the estimation error of LESO is bounded and its upper bound decreases with the observer gain [13]. However, LESO will be more sensitive to noise with higher observer gain, which should be rationally selected according to control target and characteristics of the actual system.

4.3. PID Controller with HGTD Design. In contrast to LADRC, PID controller is applied to the electric erection system. In consideration of the quantization noise of the low-resolution encoder, HGTD [24] is introduced to filter the stair-step signals of the erection angle encoder and estimate its differential signals. The structure of PID controller with HGTD is shown in Figure 9.

The expression of HGTD is

$$\begin{aligned} \dot{y}_1 &= y_2 + 2\omega_h\left(y - y_1\right) \\ \dot{y}_2 &= \omega_h^2\left(y - y_1\right) \end{aligned} \tag{21}$$

where y_1 and y_2 are, respectively, the filtered signals and the differential signals of the erection angle, and ω_h is the gain of HGTD.

Table 2: Parameters of model and Simulink configuration.

Parameters	Symbols	Values	Units
Transfer coefficient	K	20.944	$rad \cdot s^{-1} \cdot V^{-1}$
Time constant	T	0.0158	s
Reduction ratio	i	2	–
Lead of ball screw	L	0.005	m
Target position	θ	$\pi/3$ (60)	rad (deg)
Duration of erection process	t_f	10	s
Solver type	–	Fixed-step	–
Sample time	–	0.001	s

Table 3: Tuned control parameters of LADRC and PID.

Controller	Control parameters	Symbols	Values
Reduced-order LADRC	Observer gain	ω_o	10
	Coefficient of position error feedback	k_p	10
	Coefficient of velocity feedforward	k_v	1
	Coefficient of acceleration feedforward	k_a	0
Traditional LADRC	Observer gain	ω'_o	20
	Coefficient of position error feedback	k'_p	200
	Coefficient of velocity feedforward	k'_v	0
	Coefficient of acceleration feedforward	k'_a	12
PID with HGTD	Gain of HGTD	ω_h	10
	Proportional coefficient	k_P	150
	Integral coefficient	k_I	1500
	Derivative coefficient	k_D	15

The control law is expressed as

$$u_1 = k_P(\theta_r - y_1) + k_I \int (\theta_r - y_1) + k_D(\dot{\theta}_r - y_2) \quad (22)$$

where k_P, k_I, and k_D are the proportional, integral, and derivative coefficient, respectively.

5. Simulation and Experimental Verification

In order to verify the performance of the proposed controllers, simulations are conducted in MATLAB/Simulink and experiments are carried out on the experimental platform of the electric erection system, as shown in Figure 2. The control program of the experiments is written and compiled to codes in MATLAB/Simulink, which can be loaded to the GTS800 motion controller. The parameters of model and Simulink configuration are shown in Table 2.

5.1. Simulation Results and Analysis. Based on (1) and (6), the simulation model can be built in Simulink. Moreover, the stair-step signals of the low-resolution encoder caused by quantization noise can be simulated by the block—"Quantizer"—using the round-to-nearest method, according to the resolution of encoder. The tuned control parameters of LADRC and PID are shown in Table 3.

The trajectory tracking curves of reduced-order LADRC and traditional LADRC and PID with HGTD are shown in Figure 10. The tracking error is defined as the value of planned trajectory minus the simulation value without quantization noise at the same time.

From Figure 10, it can be seen that each of reduced-order LADRC, traditional LADRC, and PID with HGTD can track the planned trajectory within the required error range of $\pm 0.2^\circ$ and the terminal errors of them are almost zero. Besides, reduced-order LADRC has the highest tracking accuracy among three controllers.

Figure 11 shows the erection angle estimation error curves of second-order LESO, third-order LESO, and HGTD. The estimation error is defined as the simulation value without quantization noise minus the estimation value at the same time.

In Figure 11, the erection angle estimation error of second-order LESO can be controlled around 0°, which is the minimum among three controllers. Both third-order LESO and HGTD can control the estimation error within $\pm 0.05^\circ$, which means that the maximum error is not exceeding the resolution of the encoder. Also, according to the planned trajectory in (10), the velocity is relatively low at the beginning and end. For three controllers, at low speed, the estimation error is larger than that at high speed. Therefore, both LESO and HGTD are more sensitive to the quantization noise at low speed.

Figure 12 shows the angular velocity estimation error curves of third-order LESO and HGTD. The simulation angular velocity is obtained by calculating the differential of the simulation erection angle without quantization noise. The

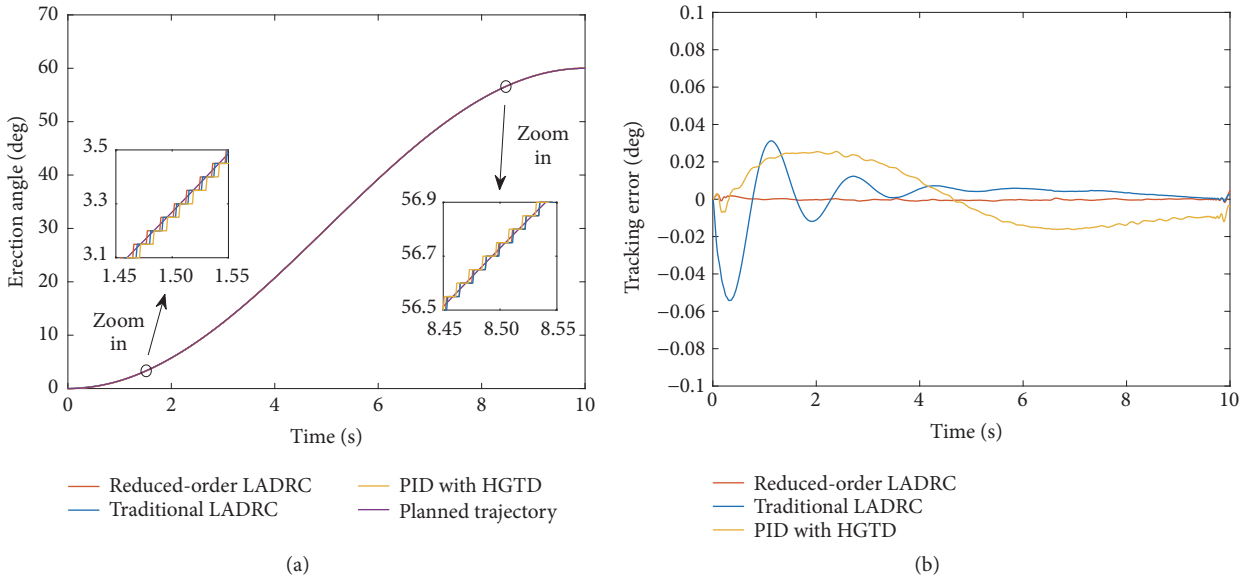

FIGURE 10: Trajectory tracking curves of reduced-order LADRC, traditional LADRC and PID with HGTD. (a) Trajectory tracking curves. (b) Tracking error curves.

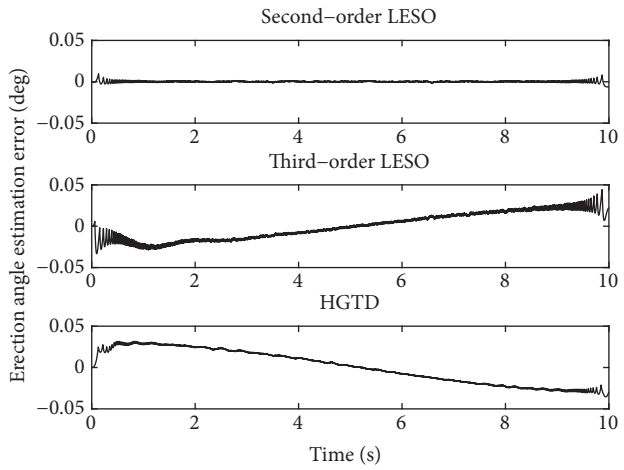

FIGURE 11: Erection angle estimation error curves of second-order LESO, third-order LESO, and HGTD.

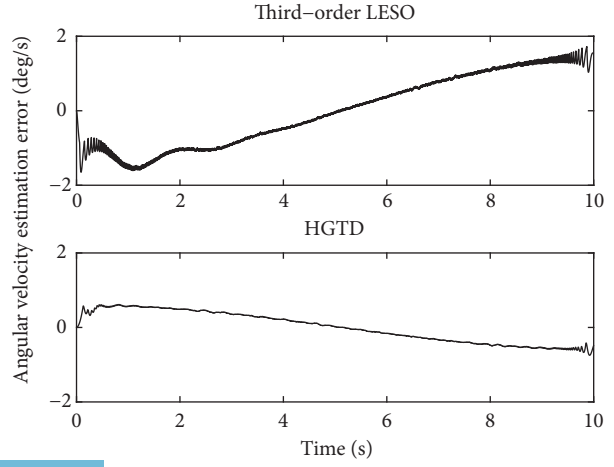

FIGURE 12: Angular velocity estimation error curves of third-order LESO and HGTD.

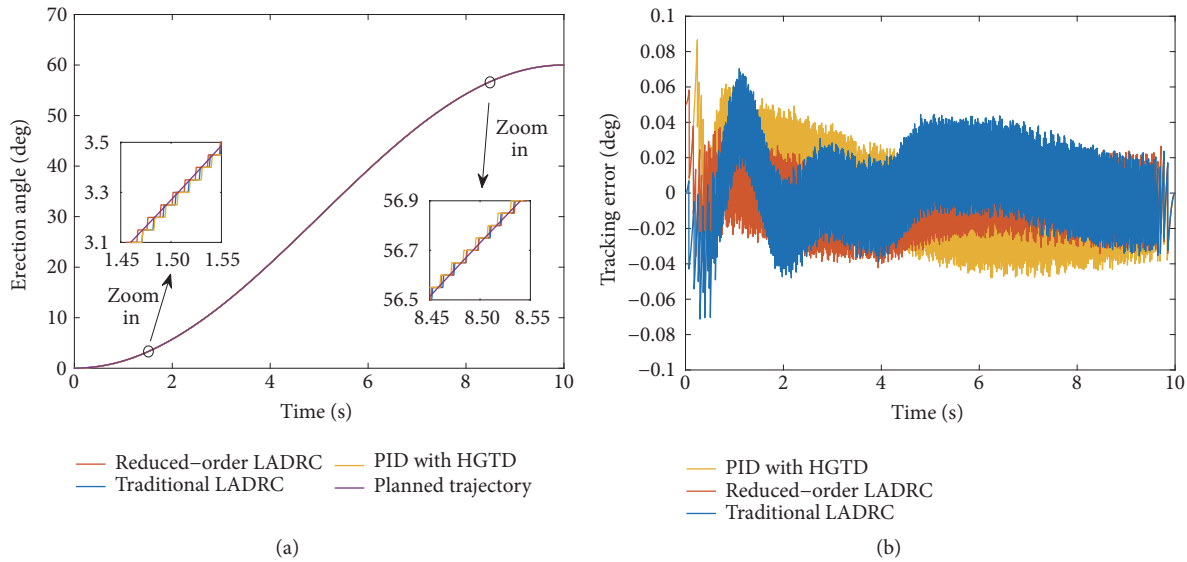

Figure 13: Trajectory tracking curves with 180 kg loads. (a) Trajectory tracking curves. (b) Tracking error curves.

Table 4: Minimum, maximum, and terminal values of tracking error.

Controller	Minimum error	Maximum error	Terminal error
Reduced-order LADRC	-0.04°	0.06°	≈0°
Traditional LADRC	-0.07°	0.07°	≈0°
PID with HGTD	-0.05°	0.09°	≈0°

estimation error is defined as the simulation value minus the estimation value at the same time.

In Figure 12, it is obvious that the angular velocity estimation error of third-order LESO is larger than that of HGTD. Also, at low speed, third-order LESO and HGTD both have larger angular velocity estimation error than that at high speed, which is similar to the erection angle estimation error.

Simulation results indicate that reduced-order LADRC, traditional LADRC, and PID with HGTD all can realize the control target for the electric erection system and reduced-order LADRC has the highest tracking accuracy. Moreover, both LESO and HGTD can filter the stair-step signals of low-resolution encoder and third-order LESO and HGTD also can estimate its differential signals, which is beneficial to improve the tracking accuracy.

5.2. Experimental Results and Analysis. The simulation results have proven that LADRC is effective and reduced-order LADRC has the highest tracking accuracy. Carrying out three controllers on the experimental platform, with the loads of 30 kg, 80 kg, 130 kg, and 180 kg, respectively, can verify their control performance in further. Besides, comparing the experimental results with the simulation results can verify the validity of the approximate model, using the same control parameters shown in Table 2

Figure 13 shows the experimental trajectory tracking curves of reduced-order LADRC, traditional LADRC and PID with HGTD, under the condition of 180 kg loads.

From Figure 13, it can be seen visually that three controllers all can keep the trajectory tracking error within the required error range of ±0.2°. Table 4 shows the Minimum, maximum, and terminal error of three controllers in the process of erection.

According to Figure 13 and Table 4, all tracking error curves of three controllers have different levels of fluctuation at the early stage of the erection process and then converge to zero, which is influenced by the low-speed performance of the servo system and the estimation performance of LESO and HGTD at low speed. Among three controllers, reduced-order LADRC has minimum fluctuation range.

Figure 14 shows trajectory tracking error curves of reduced-order LADRC, traditional LADRC and PID with HGTD, under the conditions of 30 kg, 80 kg, 130 kg, and 180 kg loads, respectively.

As presented in Figure 14(a), for reduced-order LADRC, the error range and fluctuation trend are not affected by the varying loads and the error curves are nearly the same with different loads. In Figures 14(b) and 14(c), the error curves have slight differences on the fluctuation trend, under the condition of 180 kg loads. In general, all of three controllers are robust to variation in erection loads and reduced-order LADRC has the best robustness.

Figure 15 compares the experimental trajectory tacking curves and tracking error curves of three controllers

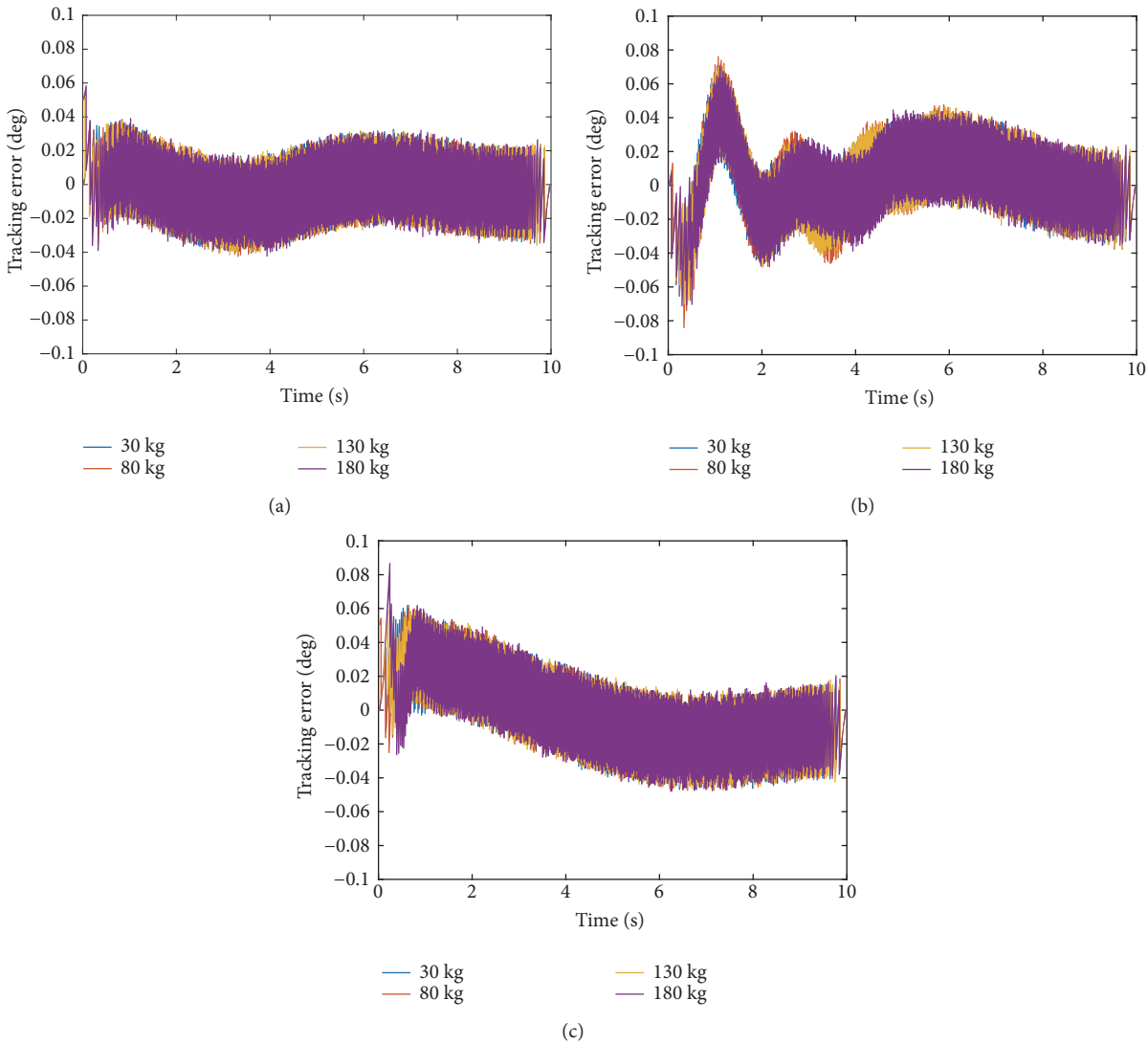

Figure 14: Trajectory tracking error curves with different loads. (a) Reduced-order LADRC. (b) Traditional LADRC. (c) PID with HGTD.

with the simulation curves, under the condition of 180 kg loads.

It can be seen from Figure 15 that, for three controllers, there is no significant difference between the experimental curves and the simulation curves. This result indicates that the approximate model of the electric erection system in Section 3 is valid to verify the control algorithm and tune control parameters.

Experimental results indicate that reduced-order LADRC can control the trajectory tracking error within the required error range with low-resolution encoder and has robustness to variation in erection loads. Compared with traditional LADRC and PID with HGTD, reduced-order LADRC has higher tracking accuracy and better robustness. In addition, the validity of the approximate system model proposed in this paper is verified by comparison of experimental curves with simulation curves.

6. Conclusions

The lever-type electric erection system in this paper is mainly composed of the servo system configured at velocity control mode and the lever-type erection mechanism. The approximate model is built by means of system identification and curve fitting. Considering the modeling uncertainties, varying loads, and the low-resolution encoder, reduced-order LADRC is proposed based on the further simplified system model. The following conclusions can be drawn based on the simulation and experimental results:

(1) For the lever-type electric erection system, reduced-order LADRC has higher tracking accuracy with low-resolution encoder and better robustness to variation in erection loads, compared with traditional LADRC and PID with HGTD.

(2) The approximate model is proved to be valid to verify the control algorithm and tune control parameters.

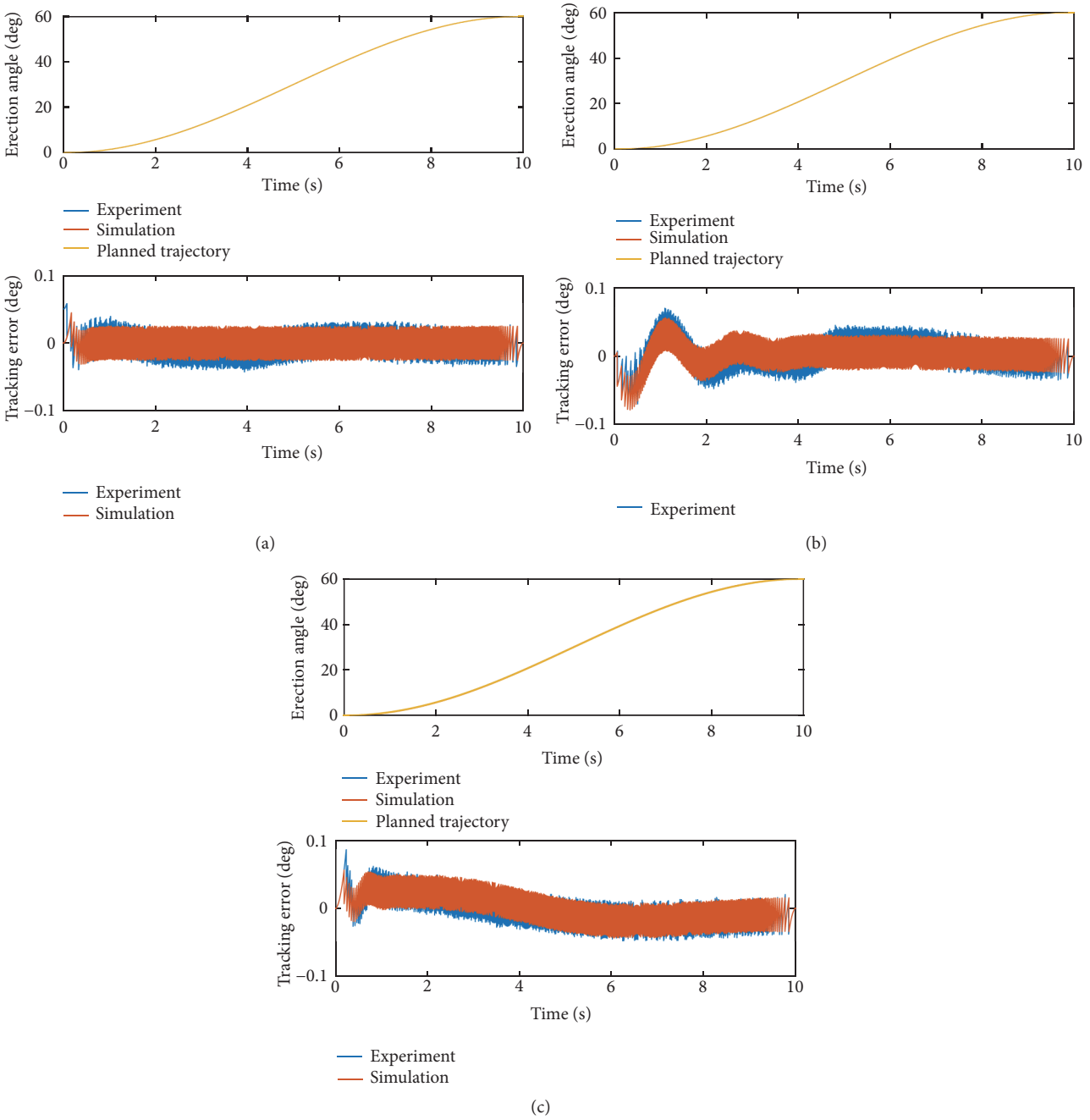

Figure 15: Comparison of experimental curves with simulation curves. (a) Reduced-order LADRC. (b) Traditional LADRC. (c) PID with HGTD.

Future research will consider the trajectory planning of this system and the optimization of the dynamic performance of this controller.

Data Availability

The data used to support the findings of this study are available from the corresponding author upon request.

Conflicts of Interest

The authors declare that there are no conflicts of interest regarding the publication of this paper.

Acknowledgments

This research was supported by the National Natural Science Foundation of China [Grant no. 61703410].

References

[1] J. Yao, Z. Jiao, D. Ma, and L. Yan, "High-accuracy tracking control of hydraulic rotary actuators with modeling uncertainties," *IEEE/ASME Transactions on Mechatronics*, vol. 19, no. 2, pp. 633–641, 2014.

[2] J. Yao, W. Deng, and Z. Jiao, "Adaptive control of hydraulic actuators with LuGre model-based friction compensation," *IEEE Transactions on Industrial Electronics*, vol. 62, no. 10, pp. 6469–6477, 2015.

[3] J. Yao, Z. Jiao, and D. Ma, "A Practical Nonlinear Adaptive Control of Hydraulic Servomechanisms with Periodic-Like Disturbances," *IEEE/ASME Transactions on Mechatronics*, vol. 20, no. 6, pp. 2752–2760, 2015.

[4] Z. Xie, J. Xie, W. Z. Du et al., "Time-varying integral adaptive sliding mode control for the large erecting system," *Mathematical Problems in Engineering*, vol. 2014, Article ID 950768, 11 pages, 2014.

[5] J. T. Feng, Q. H. Gao, Y. J. Shao, and W. X. Qian, "Flow and pressure compound control strategy for missile hydraulic erection system," *Acta Armamentarii*, vol. 39, no. 2, pp. 209–216, 2018.

[6] Y. G. Liu, X. H. Gao, and X. W. Yang, "Research of control strategy in the large electric cylinder position servo system," *Mathematical Problems in Engineering*, vol. 2015, Article ID 167628, 6 pages, 2015.

[7] J. Han, "Auto-disturbances-rejection controller and its applications," *Control and Decision*, vol. 13, no. 1, pp. 19–23, 1998.

[8] J. Q. Han, "From PID to active disturbance rejection control," *IEEE Transactions on Industrial Electronics*, vol. 56, no. 3, pp. 900–906, 2009.

[9] B. Kou, F. Xing, C. Zhang, L. Zhang, Y. Zhou, and T. Wang, "Improved ADRC for a Maglev Planar Motor with a Concentric Winding Structure," *Applied Sciences*, vol. 6, no. 12, Article ID 419, 2016.

[10] G. Herbst, "A simulative study on active disturbance rejection control (ADRC) as a control tool for practitioners," *Electronics*, vol. 2, no. 3, pp. 246–279, 2013.

[11] C. F. Fu, *Analysis and Design of Linear Active Disturbance Rejection Control [Ph.D. thesis]*, North China Electric Power University, Beijing, China, 2018.

[12] Z. Gao, "Scaling and bandwidth-parameterization based controller tuning," in *Proceedings of the American Control Conference*, pp. 4989–4996, Denver, Colo, USA, June 2003.

[13] Q. Zheng, L. Q. Gao, and Z. Gao, "On stability analysis of active disturbance rejection control for nonlinear time-varying plants with unknown dynamics," in *Proceedings of the 46th IEEE Conference on Decision and Control (CDC '07)*, pp. 3501–3506, New Orleans, La, USA, December 2007.

[14] Q. Zheng and Z. Gao, "Active disturbance rejection control: between the formulation in time and the understanding in frequency," *Control Theory and Technology*, vol. 14, no. 3, pp. 250–259, 2016.

[15] D. Yuan, X. J. Ma, Q. H. Zeng, and X. B. Qiu, "Research on frequency-band characteristics and parameters configuration of linear active disturbance rejection control for second-order systems," *Control Theory Appl*, vol. 30, no. 12, pp. 1630–1640, 2013 (Chinese).

[16] Y. Huang and W. Xue, "Active disturbance rejection control: methodology and theoretical analysis," *ISA Transactions*, vol. 53, no. 4, pp. 963–976, 2014.

[17] J. Yao and W. Deng, "Active Disturbance Rejection Adaptive Control of Hydraulic Servo Systems," *IEEE Transactions on Industrial Electronics*, vol. 64, no. 10, pp. 8023–8032, 2017.

[18] J. Yao, Z. Jiao, and D. Ma, "Adaptive robust control of dc motors with extended state observer," *IEEE Transactions on Industrial Electronics*, vol. 61, no. 7, pp. 3630–3637, 2014.

[19] Y. Zheng, D. W. Ma, J. Y. Yao, and J. Hu, "Active disturbance rejection control for position servo system of rocket launcher," *Acta Armamentarii*, vol. 35, no. 5, pp. 597–603, 2014.

[20] D. Qiu, M. Sun, Z. Wang, Y. Wang, and Z. Chen, "Practical wind-disturbance rejection for large deep space observatory antenna," *IEEE Transactions on Control Systems Technology*, vol. 22, no. 5, pp. 1983–1990, 2014.

[21] D. Wu, T. Zhao, and K. Chen, "Research and industrial applications of active disturbance rejection control to fast tool servos," *Control Theory Appl*, vol. 30, no. 12, pp. 1534–1542, 2013.

[22] Y. Liu, Q. Gao, H. Niu, and X. Cheng, "Modeling and trajectory planning of leveraged balance on lifting mechanism," *Journal of Vibration and Shock*, vol. 36, no. 16, pp. 212–217, 2017.

[23] Z. W. Xu, J. P. Jiang, and Z. F. Luo, "Permanent magnet synchronous motor position servo system controlled by fuzzy model algorithmic control," *Transaction of China Electrotechnical Society*, vol. 18, no. 4, pp. 99–102, 2003.

[24] H. Feng and S. Li, "A tracking differentiator based on Taylor expansion," *Applied Mathematics Letters*, vol. 26, no. 7, pp. 735–740, 2013.